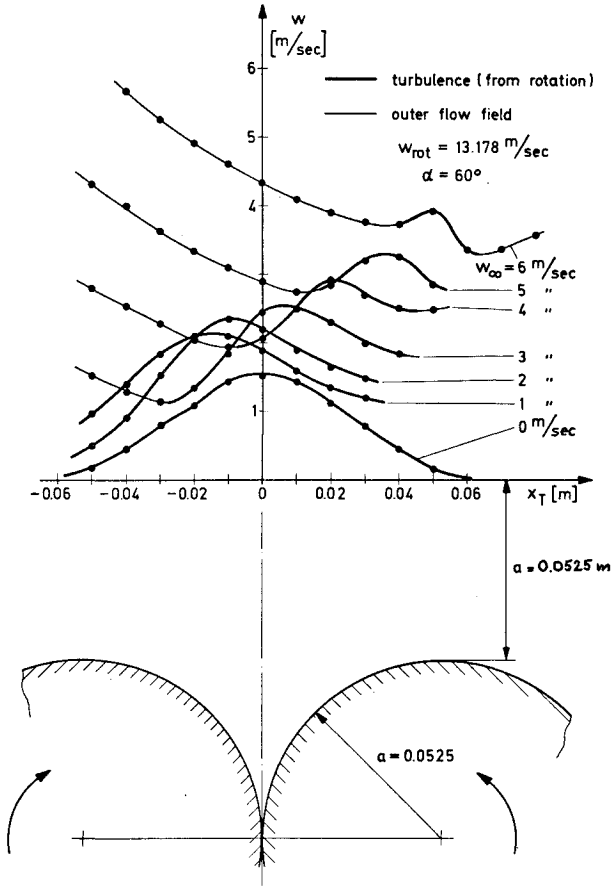


**Fig. 7 Velocity distribution behind the rotating cylinders, measured with hot wire probes.**

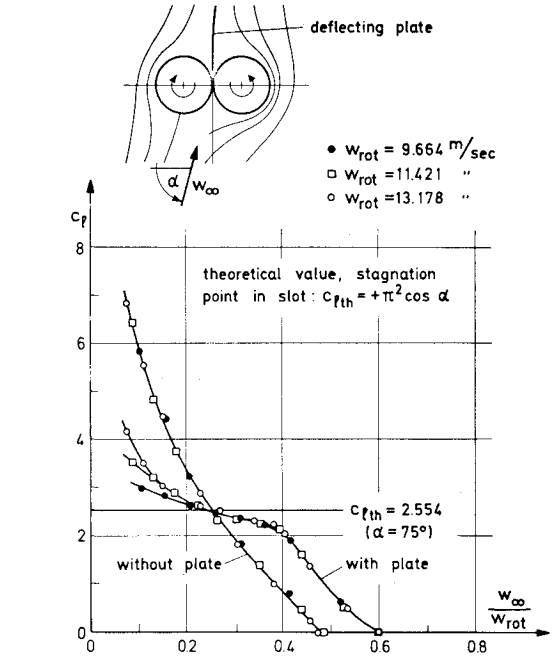


**Fig. 8 Influence of a deflecting plate behind the cylinders. The theoretical values for $\varphi_r$ = 180 deg can be achieved.**

stagnation point located in the slot between the two cylinders as shown in Fig. 3. This condition is valid for one ratio $w_\infty / w_{rot}$ only and is therefore not generally applicable. In the region of 52.5 deg $\leq \alpha \leq$ 90 deg (lefthand side of Fig. 6), no pressure drag was measured for $w_\infty / w_{rot} \leq 0.40$. In the case of $\alpha = 90$ deg where no lift force is generated, the optimum velocity ratio based on the drag measurements was $w_\infty / w_{rot} = 0.405$.

The lift coefficients $c_l$ in the region 0 deg $\leq \alpha \leq$ 45 deg (righthand side of Fig. 6) show a different behavior indicating that viscous forces degrade the lift-to-drag ratio of the cylinders. Large portions of the cylinder walls move against the general flow direction causing local flow separations to occur. At $\alpha < 75$ deg the measured lift exceeded the maximum theoretical value of $c_{l_{th}} = 9.87$. However, the measurements at the corresponding very low ratios $w_\infty / w_{rot}$ are not so accurate due to the low flow velocity (on the order of 1 m/s or less). Of course the jet formed by the cylinder boundary layer should cause some additional lift.

In order to understand the flow conditions at the rear stagnation point the velocity distribution behind the cylinders was measured with hot wire probes (Fig. 7). The profile of the jet for different flow velocities shows a distinct displacement to the right towards the freestream flow direction when $w_\infty$ is increased. At low free stream velocities the jet determines the location of the outgoing streamline and thereby the whole flowfield. This is confirmed by tests with a deflecting plate attached to the wind tunnel wall and located just behind the cylinders (Fig. 8).

The curve is approaching the theoretical value $c_{l_{th}} = 2.554$ for decreasing $w_\infty / w_{rot}$ with the exception of very low ratios of $w_\infty / w_{rot}$, where again the jet produced by the rotating cylinders dominates the flow.

## Concluding Remarks

The flow around two rotating cylinders inclined to the flow direction is governed by the jet formed by the boundary layers on the two cylinders and associated interaction with the external flowfield. For velocity ratios $w_\infty / w_{rot} \leq 0.4$ and for angles of attack 90 deg $< \alpha <$ 52.2 deg, the tests indicate a greatly reduced or eliminated pressure drag.

A new concept of stagnation point control is demonstrated that is not based upon avoiding flow separation (the Kutta-Joukowski condition) as on the single rotating cylinder, but rather depends on the effect of the momentum of the two boundary layers of the rotating cylinders forming a jet that defines the downstream flow conditions.

## References

[1] Bridel, G., and Thomann, H.H., "Wind Tunnel Balance Based on Piezoelectric Quartz Force Transducers," *Journal of Aircraft*, Vol. 17, May 1980, pp.

[2] Bridel, G., "Strömungsuntersuchungen an 2 rotierenden Zylindern mit einer neuen Mehrkomponentenwaage," Thesis No. 6108, Swiss Federal Institute of Technology, Zurich, Switzerland.



# Aircraft Configuration Optimization for Ground Attack Mission

P. Ramamoorthy* and A. K. Sinha*
*National Aeronautical Laboratory, Bangalore, India*

| | |
|---|---|
| $AR$ | = wing aspect ratio |
| $C_{D_0}$ | = profile drag coefficient |
| $C_{D_B}$ | = base drag coefficient |
| $C_{D_F}$ | = skin friction drag coefficient |
| $C_{D_W}$ | = wave drag coefficient |
| $C_L$ | = lift coefficient |

Received Aug. 20, 1979. 

Index categories: Configuration Design; Performance; Aerodynamics.

*Scientist, Aerodynamics Division.

$H$ = cruise altitude, m
$K$ = lift induced drag coefficient
$M, M_\infty$ = freestream Mach number
$P$ = ambient pressure, kg/m$^2$
$R$ = radius of action, n. miles
$R_{e\bar{c}}$ = Reynolds number based upon mean aerodynamic chord
$S$ = wing gross planform (reference area, m$^2$)
SEP = specific excess power, m/min
sfc = specific fuel consumption, kg/kg-h
$T$ = ambient temperature, K
THRUST = net thrust, kg
TOD = takeoff distance, m
$t/c$ = wing thickness ratio
$W$ = all-up-weight, kg
$W_{D_F}$ = wave drag factor (ratio of wave drag of the whole aircraft to that of Adam's body at $M = 1.2$)
$W/S$ = wing loading, kg/m$^2$
$V_{max}$ = maximum level speed, knots
$V_{min}$ = minimum level speed, knots
$V_{stall}$ = stall speed, knots
$\Lambda$ = wing leading edge sweep, deg
$\lambda$ = wing taper ratio

## Introduction

THE task of designing a new aircraft consists essentially of finding the optimum practical combination of configuration variables to achieve the design objective with known constraints. The design objective in case of a military aircraft is stated in the form of Air Staff Requirement. Generally, ASR is spelled out in terms of both point and mission performances together with specification of navigational, weapon, and control systems. The required point performance could be minimum radius of turn or maximum load factor at any given altitude, speed, and thrust setting or best rate of climb with a desired speed. Again, the mission performance is expressed as the capability of delivering a given war load over as far a distance as possible with a given amount of fuel and flying in a given profile.

In this paper, we have tried to obtain the optimal combination of wing planform variables, wing thickness ratio, and wing loading to achieve the maximum radius of action for given amount of fuel and armament. The design variables are constrained to remain within given lower and upper bounds while takeoff distance and all-up-weight are constrained to be less than given values. The fuselage and empennage geometry and the engine were assumed to be frozen. It is further assumed that the optimum planform and the given fuselage will be able to accommodate the armament and fuel. The mission for which the optimization is carried out is given in Fig. 1.

The results of this study are extremely interesting and provide a basis for optimizing the wing of an aircraft at least for its primary role. More work incorporating the secondary missions, more design variables characterizing the fuselage

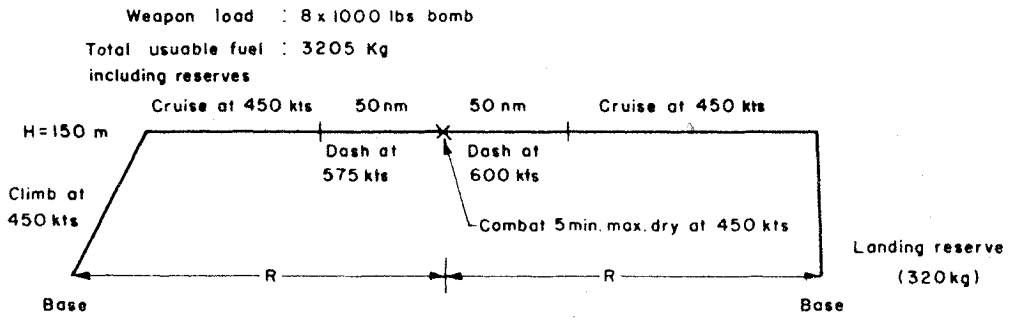


Fig. 1 Low level ground attack role.

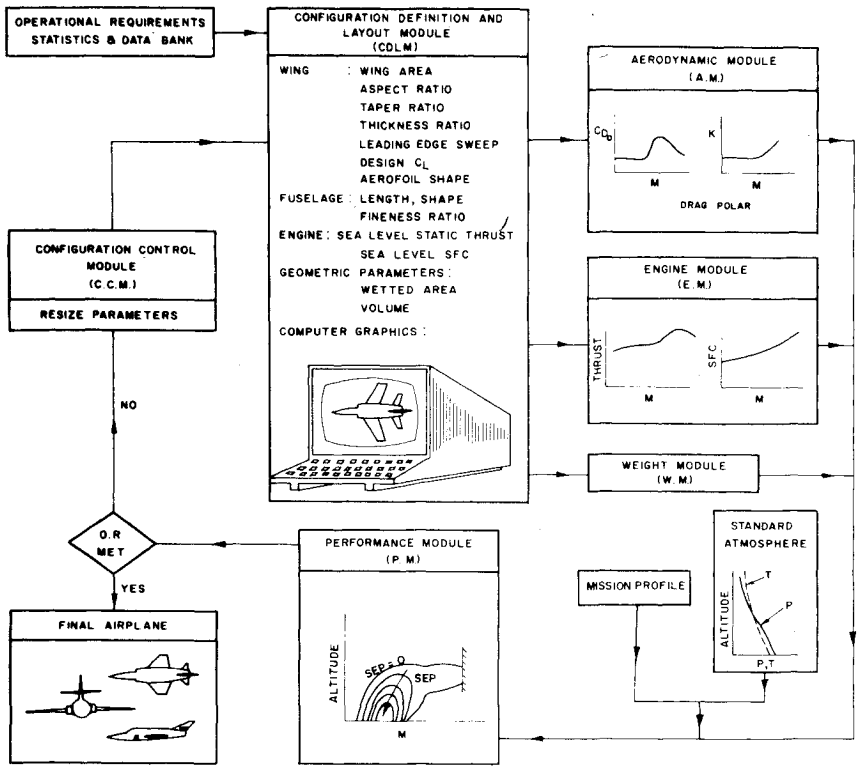


Fig. 2 Flow chart for aircraft configuration optimization.

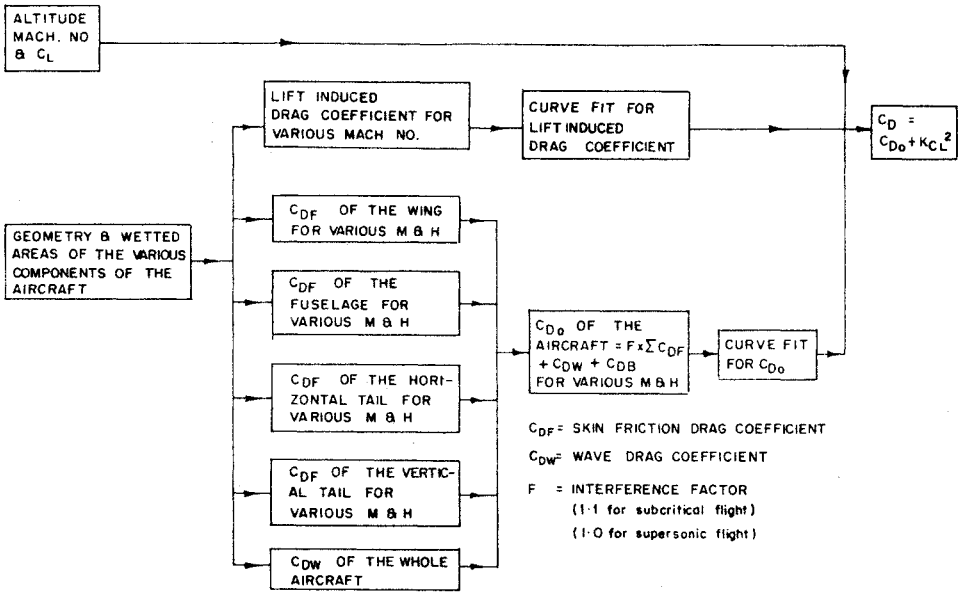


**Fig. 3 Flow chart for aerodynamic module.**

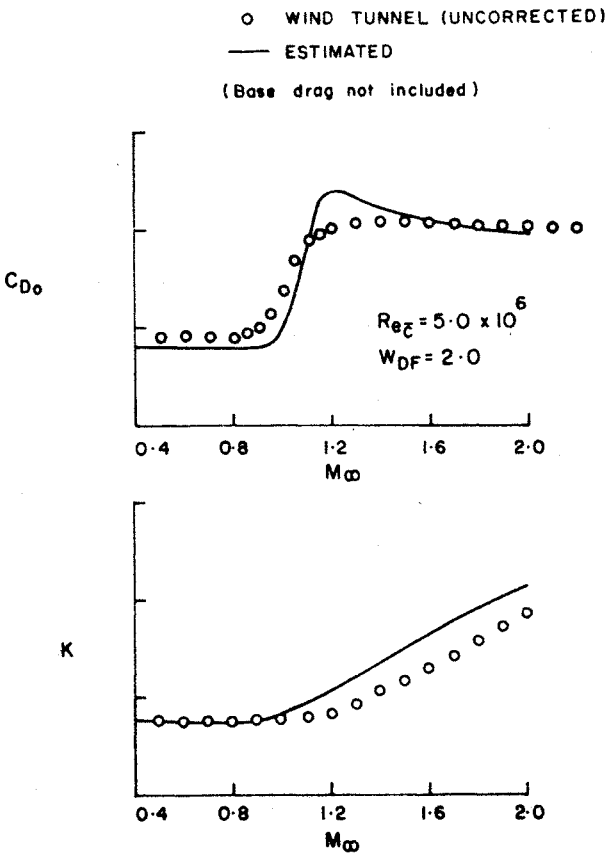


**Fig. 4 Comparison of results obtained by AM with experiments.**

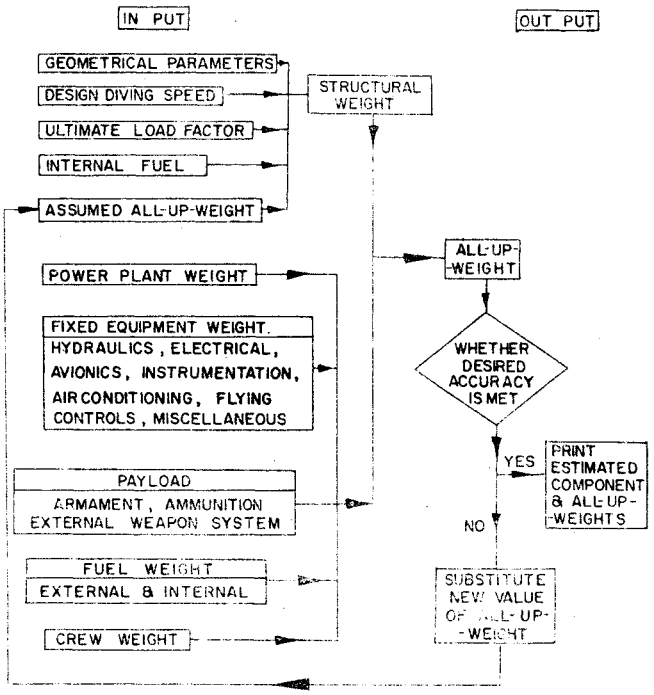


**Fig. 5 Flow chart for weight module.**

and empennage, and the inclusion of more engineering constraints are called for before the methodology could be finalized. Hooking this optimization procedure with an interactive graphic display software makes the design venture more sophisticated and realistic. These are some of the areas of study under progress.

In the next section the procedure adopted for optimization is given which is followed by the section containing results and discussions.

## Procedure

The general procedure for optimization is illustrated in Fig. 2. Starting from any arbitrary configuration, the wetted areas, volumes, and other geometrical quantities are estimated from the basic independent configuration variables in the configuration definition and layout module (CDLM). This module has the option of calling a graphic subroutine to display the wing planform and hence the way it is changing from iteration to iteration when used in conjunction with an interactive graphic terminal. Aerodynamic module (AM) accepts the input from the CDLM and evaluates the aerodynamic characteristics ($C_{D_0}$ and $K$) for different altitude and Mach number, mainly from semiempirical methods.[1] The flow chart for AM is given in Fig. 3. A typical comparison of wind tunnel values of $C_{D_0}$ and $K$ for an aircraft model with results obtained by AM is given in Fig. 4. In the weight module (WM), structural weight is estimated by empirical formulas knowing the geometric parameters, ultimate load factor, and design diving speed. Weight of the engine is assumed to be known (otherwise it can be calculated by regression analysis of similar engines knowing the sea level static thrust). Fuel weight is given (or it can be calculated from

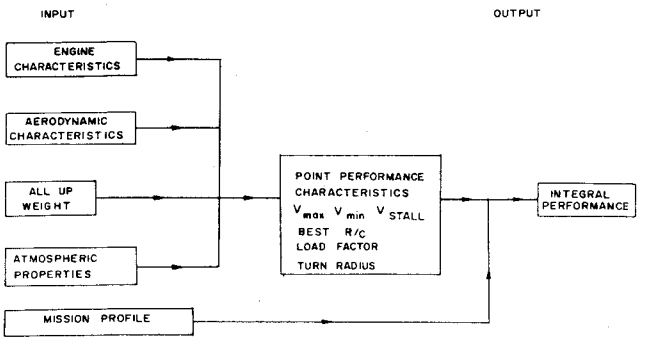


**Fig. 6 Flow chart for the performance module.**

**Table 1 Design parameters for starting and optimum wing configurations**

| Parameters | Starting wing | Optimized wing |
|---|---|---|
| Aspect ratio $\mathcal{R}$ | 2.9 | 3.1 |
| Leading edge sweep, $\Lambda$ deg | 50 | 45 |
| Taper ratio $\lambda$ | 0.212 | 0.201 |
| Thickness ratio $t/c$ | 0.06 | 0.06 |
| Span $b$, m | 8.76 | 8.80 |
| Ref. area $S$, m$^2$ | 26.55 | 25.35 |
| Center line chord $C_0$, m | 5.0 | 4.8 |
| Tip chord $C_t$, m | 1.06 | 0.96 |
| Wing loading $W/S$, kg/m$^2$ | 506 | 528 |
| [a] All-up-weight $W$, kg | 13,447 | 13,391 |
| [a] Takeoff distance TOD, m | 1460 | 1499 |
| [a] Radius of action $R$, n. miles | 178 | 183 |

[a] These numbers do not reflect the accuracies involved in the procedures used in computing these quantities.

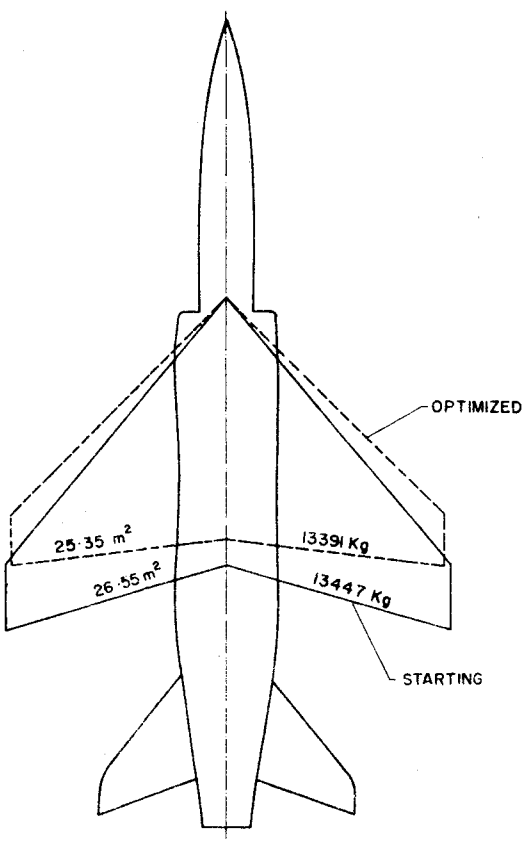


**Fig. 7 Existing and optimum configurations.**

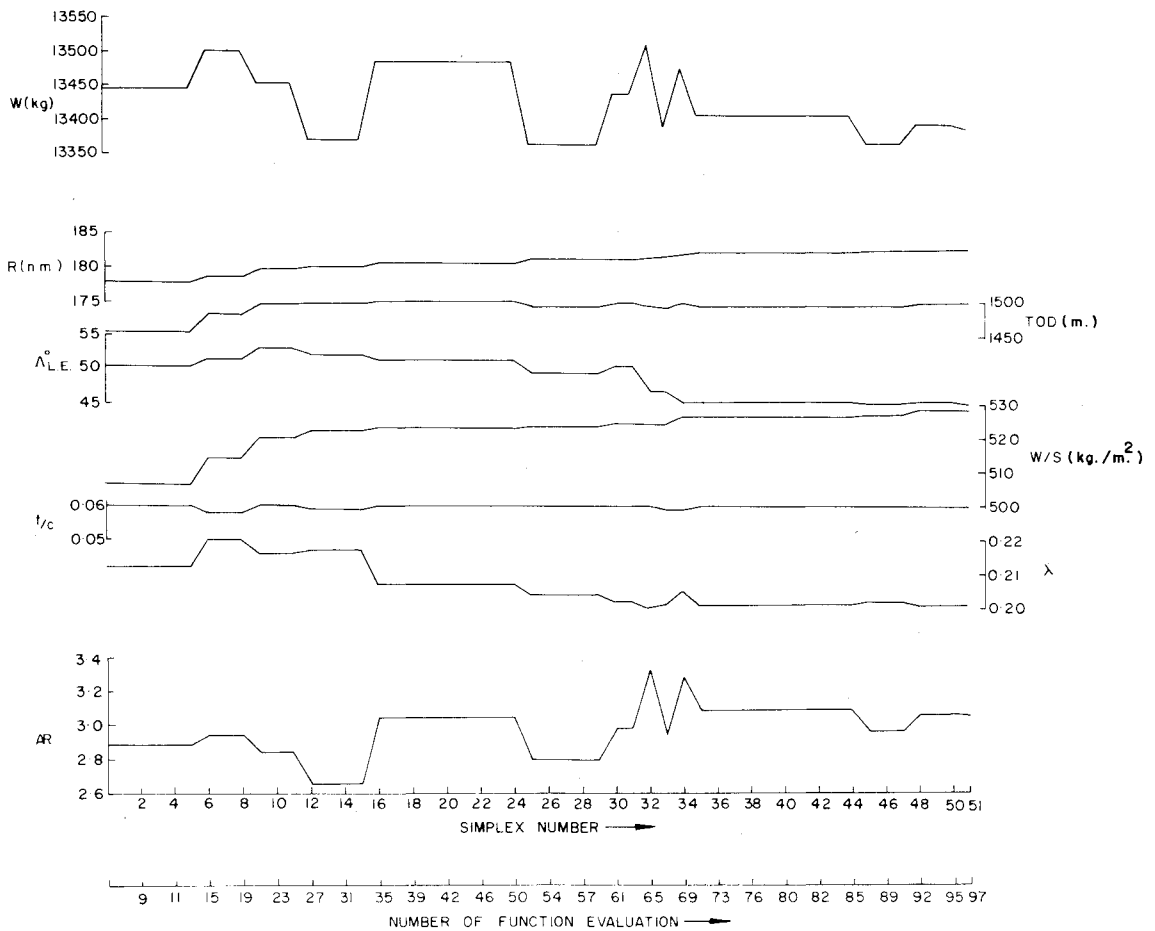


**Fig. 8 Variation of design parameters with function evaluation.**

the formula for range if range is given). Adding payload, systems weight, and crew weight to all the above weights, one gets the all-up-weight. Iteration is involved to obtain the all-up-weight. Figure 5 gives the flow chart for the WM. In this problem the engine module (EM) consists of the data bank of thrust and sfc for various altitudes and Mach numbers of an existing engine around which the aircraft is designed. Performance module (PM) accepts the values obtained from AM, WM, and EM as input together with mission profile (Fig. 1) and properties of the standard atmosphere and computes the required point performance parameters and radius of action.[2] Figure 6 gives the flow chart of PM. The configuration control module (CCM), which essentially is a multivariable search for optimum of a given cost function, viz. radius of action, under design and operational constraints, adjusts the design parameters in each iteration until the optimum is reached. In the mathematical programming language the above procedure can be expressed as:

Maximize $R(X)$ with $X_L \leq X \leq X_U$, $W \leq 14{,}000$ kg, $TOD \leq 1500$ m and where $R$ = radius of action in n. miles, and

$$X = \begin{bmatrix} AR \\ W/S \\ \Lambda \text{ deg} \\ \lambda \\ t/c \end{bmatrix} \quad X_L = \begin{bmatrix} 2 \\ 250 \\ 45\text{deg} \\ 0.2 \\ 0.04 \end{bmatrix} \quad X_U = \begin{bmatrix} 4 \\ 700 \\ 55 \text{ deg} \\ 0.4 \\ 0.06 \end{bmatrix}$$

In CCM, the program SWIFT (Sequential Weightage Increasing Factor Technique),[3] which is based on flexible polyhedron method for unconstrained optimization, is used. This is essentially a penalty function method which does not need a feasible starting point.

## Results and Discussion

Table 1 gives the design parameters of the starting and the optimum wings. Figure 7 shows them superimposed. Figure 8 gives the variation of design parameters with simplex number.[3] It is seen that the optimum configuration is able to increase the radius of action by 5 n. miles without compromising on the constraints. This means that the starting configuration was already near optimum. Hence the marginal increase in radius of action should be viewed in that light. What is significant is that the procedure given in this paper would lead to the optimum regardless of the starting configuration. In this case it is observed that the variation of radius of action near optimum is relatively small over a rather wide range of configuration variables excepting the wing loading. It may be noted that the primary emphasis of the study is the development of the methodology for isolating optimum configurations rather than getting larger radius of action in a quantitative sense. It might also be noted from Fig. 8 that the radius of action is a weak function of thickness ratio and as such for further optimization this variable can be neglected. Also, it is clear from Fig. 7 that the optimum wing is structurally more acceptable than the starting configuration. Floating more variables describing fuselage and empennage and inclusion of more constraints are under study.

## Acknowledgment

We thank Dr. C. L. Narayana for providing the program for predicting the aerodynamic characteristics of an aircraft, B. V. Sheela for providing the multivariable search program, "SWIFT" and G. S. Dwarakanath for helping us in troubleshooting and offering constructive criticism. We are grateful to M. Shivakumara Swamy who has consistently helped us with his useful suggestions in this work.

## References

[1] Ramamoorthy, P., Narayana, C.L., and Vimala Dutta, "Estimation of Drag Polar," National Aeronautical Laboratory Tech. Memo AE-TM-14-77, Aug. 1977.

[2] Sinha, A.K. and Ramamoorthy, P., "General Purpose Aircraft Performance Estimation Program," National Aeronautical Laboratory Tech. Memo AE-TM-79, April 1979.

[3] Sheela, B.V. and Ramamoorthy, P., "SWIFT—A New Constrained Optimization Technique," *Computer Methods in Applied Mechanics and Engineering*, Vol. 6, No. 9, 1975.

C80-094

# Effect of Adding Structural Damping on a Wing/Nacelle Hump Type Flutter Mode

80001
80006

Dave Gimmestad*
*Boeing Military Airplane Company, Seattle, Wash.*

## Introduction

ALTHOUGH it has long been known that adding structural damping suppresses some flutter modes, only recently has the materials technology progressed so that you can easily build structural damping into your airplane. These damping materials include viscoelastomers, silicones, high damping epoxies and enamels, which may be integral to the structure, or may be an add-on to the basic design. In this study the effect of adding damping to nacelle strut side bending on a wing/nacelle hump type flutter mode problem is shown.

## Discussion

A twin engine preliminary design was used in this study. The airplane has high bypass fan engines strut mounted on the wing. Damping was added to the nacelle strut in side bending. The nacelle frequency dependent characteristics were mapped with a variation on nacelle side bending stiffness, performed with and without added damping. This "chimney" effect results from the nacelle functioning as a tuned mass damper on the wing. Adding damping to the nacelle strut modifies its behavior from that of a tuned mass damper to a tuned viscoelastic damper. In this study the added damping level selected ($\eta = 0.1$), is typical of the loss factors that may be achieved with add-on damping tape treatments. Higher levels of damping are possible with damping which is designed integral to the structure.

The flutter analysis used in this study was a conventional branch modes analysis. It had 20 deg of freedom; including 6 wing bending modes, 4 wing torsion modes, 2 wing fore and aft bending modes, fore and aft body bending, 3 symmetric rigid body modes, and 3 modes of nacelle motion with respect to the wing. The added damping occurs only in the nacelle side bending generalized coordinate.

## Results

The flutter speeds of the chimney are shown as a function of nacelle side bending mode natural frequency on Fig. 1. The

Received May 2, 1979; revision received Sept. 4, 1979. 

Index categories: Aeroelasticity and Hydroelasticity; Structural Dynamics.

*Specialist Engineer.